Low-frequency plasma oscillations at Mars during the October 2003 solar storm

J. R. Espley,[1] P. A. Cloutier,[1] D. H. Crider,[2] D. A. Brain,[3] and M. H. Acuña[4]

Received 30 November 2004; revised 4 March 2005; accepted 15 March 2005; published 11 August 2005.

[1] The powerful x-class flare which occurred on the Sun on 28 October 2003 had important effects on plasma environments throughout the solar system. We present here observations of the effects at Mars from the Mars Global Surveyor (MGS) Magnetometer/Electron Reflectometer experiment. In particular we focus on the changes in the nature of the magnetic oscillations observed at an altitude of 400 km (MGS's current orbital altitude) during the passage of the solar storm. We find that strong, regular oscillations are observed in both the $B_{\|}$ and $B_{\perp}$ components of the magnetic field at all solar zenith angles. We emphasize in particular the powerful, coherent oscillations observed in the normally quiet nightside region. These oscillations carry power at the proton gyrofrequency and at and below the oxygen gyrofrequency. This implies that ions of planetary origin are interacting with the solar wind plasma and raises the possibility that significant atmospheric loss may occur during the passage of large solar storms at Mars.

Citation: Espley, J. R., P. A. Cloutier, D. H. Crider, D. A. Brain, and M. H. Acuña (2005), Low-frequency plasma oscillations at Mars during the October 2003 solar storm, *J. Geophys. Res.*, *110*, A09S33, doi:10.1029/2004JA010935.

1. Introduction

[2] The October–November solar storms produced a variety of phenomena across the solar system as documented in this special issue. *Crider et al.* [2005] use observations from Mars Global Surveyor (MGS) to show that the plasma interaction region at Mars is compressed during the passage of the coronal mass ejection (CME) that was launched from the Sun on 28 October 2003. In this work, we focus our attention on MGS observations (at an altitude of 400 km) of changes in the magnetic oscillations observed at Mars. In particular, we find that a wide variety of oscillations occur in the normally tranquil magnetotail and that in some instances, the character of the oscillations in the dayside magnetic pileup region (MPR) changes during the passage of the storm.

[3] Mars lacks a global dipole magnetic field and so, unlike planets like the Earth which have large-scale magnetospheres, the solar wind interacts directly with the Martian ionosphere, which provides the obstacle to stand off the solar wind as it flows by [*Acuña et al.*, 1998; *Cloutier et al.*, 1999]. This interaction produces a bow shock as the supersonic solar wind is slowed to subsonic speeds, a region of shocked solar wind plasma called the magnetosheath, and a lower plasma boundary called the magnetic pileup boundary (MPB) [*Vignes et al.*, 2000] where the solar wind's magnetic field is draped across the boundary produced by the ionospheric plasma via the mechanism of electron impact ionization [*Crider et al.*, 2000]. The region below the MPB is called the magnetic pileup region (MPR) and has its lower boundary in the photoelectron boundary (PEB), where the majority of the electron spectra are characteristic of electrons of planetary origin and which is therefore probably associated with the ionopause [*Mitchell et al.*, 2000]. A region sometimes called the tail or magnetotail is present on the nightside below the MPB, although a distinct boundary between the nightside MPR and the tail has not been identified. Figure 1 shows a schematic diagram (approximately to scale) illustrating the regions and boundaries just enumerated.

[4] *Espley et al.* [2004] used MGS observations to characterize the general character of low-frequency oscillations in the near Mars space. They determined that the dayside magnetosheath is dominated by mirror mode waves, that the nightside magnetosheath is dominated by resonance cyclotron waves created by the interaction of the solar wind plasma with plasma of planetary origin, and that the nightside MPR and tail region contain relatively little oscillatory activity. We compare this general picture to the dramatic changes observed during the passage of the solar storm.

2. Data Set

[5] MGS arrived at Mars in 1997 and since that time the Magnetometer/Electron Reflectometer (MAG/ER) investigation has been returning a steady flow of data [*Acuña et al.*, 2001]. When MGS first arrived at Mars it began a slow process of aerobraking in order to circularize its orbit.

[1]Department of Physics and Astronomy, Rice University, Houston, Texas, USA.
[2]Department of Physics, Catholic University of America, Washington, D.C., USA.
[3]Space Sciences Laboratory, University of California, Berkeley, Berkeley, California, USA.
[4]NASA Goddard Space Flight Center, Greenbelt, Maryland, USA.

0148-0227/05/2004JA010935$09.00

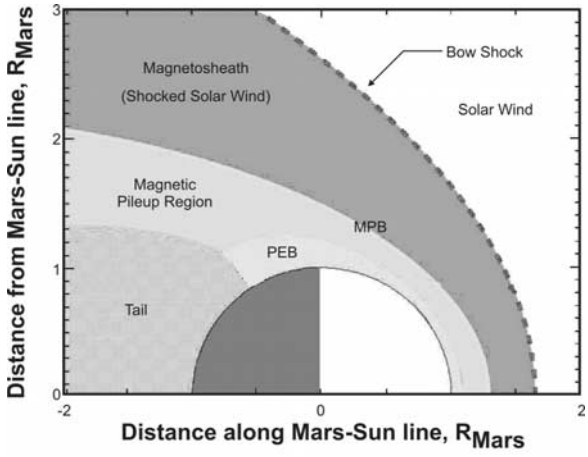

Figure 1. A schematic diagram (approximately to scale) illustrating the regions of the Martian interaction with the solar wind. Not shown are the complications introduced by the crustal magnetic field sources. The MPB is the magnetic pileup boundary and the PEB is the photoelectron boundary. Adapted from *Crider et al.* [2003]. See color version of this figure at back of this issue.

During these "premapping" phases of the mission, MGS sampled a large variety of altitudes and solar zenith angles (SZAs) as its elliptical orbit was gradually brought down to the circular mapping orbit which it reached in February of 1999 [*Albee et al.*, 2001]. All data returned since that time have been from the near circular mapping orbit which has an approximate altitude of 400 km, an orbital period of 2 hours, and covers 0200 to 1400 in local time. Hence the data we use in this study are confined to this narrow altitude range, unlike the study of *Espley et al.* [2004] which was able to use premapping data to cover large spatial regions.

[6] The MAG instrument returns high time resolution vector magnetic field data at a rate of 8, 16, or 32 samples per second. However, better calibrated lower time resolution data are available with a time resolution of 1/24th of the high time resolution data. These low time resolution data record the absolute data value rather than simply the difference between measurements recorded by the high time resolution data [*Acuña et al.*, 2001]. Therefore for calculations that require accurate absolute measurements, we use the lower time resolution data and for calculations that require only relative measurements (e.g., frequency analyses and deviations from the mean magnetic field) we use the high time resolution data.

[7] The ER instrument measures electron fluxes every 2 to 48 s across 30 energy channels ranging from 10 eV to 20 keV in 16 geometrically separate sectors. Because we are interested primarily in the relative densities of electrons in order to compare them to the fluctuations in the magnetic field, we use the omnidirectional flux of the electrons in one of the energy bins (the 191 eV bin) with the highest time resolution.

[8] The MGS data used in the study are given (prior to the data processing described below) in the Sun-state (SS) Cartesian coordinate system. In this system, the Mars-Sun line is defined as the +x direction, the orbital motion of Mars is the −y direction, and the +z axis completes the orthogonal set (and is roughly northward on Mars). This system could also be called the Mars solar orbital (MSO) system since it is comparable to the geocentric solar ecliptic (GSE) and the Venus solar orbital (VSO) coordinate systems.

3. Analysis Methods

[9] The most basic step in many of the analysis methods used in this study is the determination of the mean magnetic field for a given interval. We determine the magnitude and direction of this mean field and then rotate the MAG data into a coordinate system that is aligned along this mean field (MF). In this MF coordinate system, the principal direction is defined as the direction of the mean magnetic field over some given time interval ($B_{\|}$), the second direction is perpendicular to the mean field and contains no z-component from the SS measurements ($B_{\perp 1}$), and the third direction is perpendicular to the other two directions ($B_{\perp 2}$). Perturbations from the mean field can then be calculated in each of these directions for every measurement within the time interval.

[10] Determining the appropriate length for this time interval is one of the difficult issues with this analysis method. Because our measurements are made by a moving spacecraft, one of the dangers in interpreting perturbations in observed parameters is that we may be simply passing through a variety of plasma regimes with different characteristics rather than observing intrinsic wave structures. Conversely, if we were to use too short of a time interval, we would be excluding wave modes that have characteristic periods larger than our chosen time interval. With these guidelines in mind, in previous work [*Espley et al.*, 2004] when we have undertaken statistical analyses, we use an interval of 60 s. This is long enough to include several oscillations at the expected characteristic frequencies (the proton and oxygen gyrofrequencies) but short enough so that MGS has only moved approximately 200 km during the interval. In the present work, since we confine ourselves to analysis of individual case studies (such as shown in the results section), we often use intervals longer than 60 s, but this is because a qualitative inspection of the data permits us to determine where dramatic plasma changes occur and we are able to limit ourselves to regions that do not contain such changes. As one last step in this process, we remove any linear trends in the transformed vector components, since these types of long period changes are the type of trends we are trying to avoid by choosing a sufficiently short time interval.

[11] These transformed vector magnetic field measurements then allow us to calculate, for the interval, the average amplitudes of the fluctuations in a given direction and the ellipticity of the perpendicular components (the ellipticity is 0 if the oscillations are perfectly linear and 1 if they are perfectly circular). We also calculate the average sense of polarization of the fluctuations about the mean field (where left-handed polarization corresponds to the motion of ions in a magnetic field and right-handed polarization to the motion of electrons).

[12] Another analysis technique that we use is the comparison of fluctuations in the magnetic field to the fluctua-

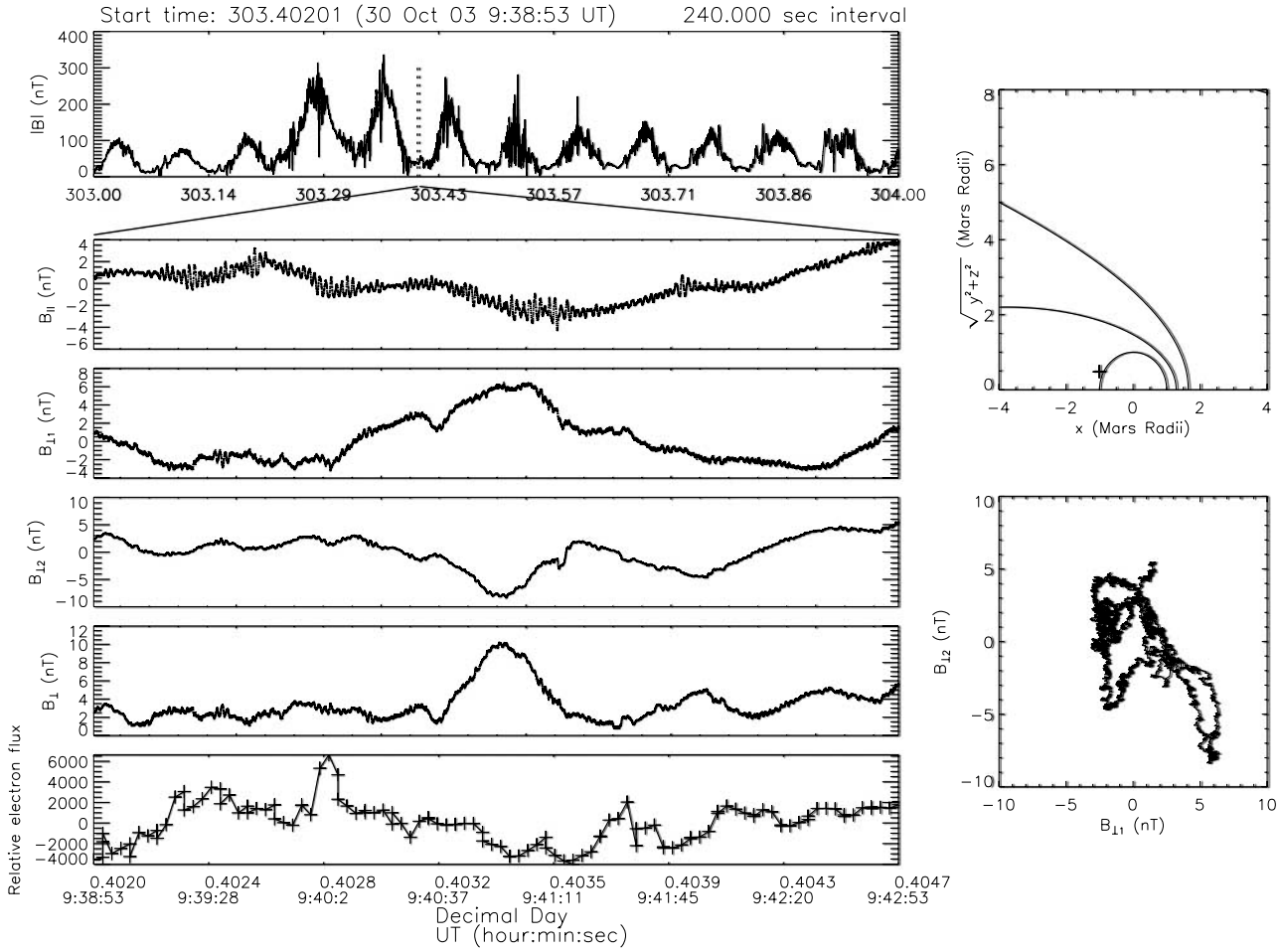

Figure 2. A detailed analysis of the interval from decimal day 303.402 to 303.405 (30 October 2003). (top left) The $|B|$ time profile for the entire day with dashed lines indicating the interval of interest analyzed below. (left panels from second to top to bottom) These panels show the $B_{\|}$, $B_{\perp 1}$, $B_{\perp 2}$, $B_{\perp}$ components, and relative electron flux for the interval of interest. (top right) The starting and stopping locations of MGS (shown as plus symbols) during the interval analyzed in SS coordinates. Also shown are the best fit bow shock and MPB curves. (bottom right) The hodogram of the $B_{\perp}$ components for the interval.

tions in the ER flux data. We first find the relative fluctuations in the omnidirectional flux of the 191 eV electrons (cf. section 2) for a given interval. Again, we linearly detrend the data to remove undesired large-scale changes. We then find the Spearman correlation coefficients between these fluctuations and the fluctuations in $B_{\|}$ and the fluctuations perpendicular to the mean magnetic field ($B_{\perp}$ where $B_{\perp} = B_{\perp 1} + B_{\perp 2}$). The Spearman coefficient is a nonparametric correlation coefficient that is 1 if the two time series are perfectly correlated, 0 if they are perfectly noncorrelated, and -1 if they are perfectly anticorrelated [*Press et al.*, 1992].

[13] In order to determine possible directions of propagation (or in the case of stationary structures the direction of the wave vector), we use minimum variance analysis (MVA) which works by solving for the eigenvector of the covariance matrix which corresponds to the direction of minimum variance [*Song and Russell*, 1999]. This direction is then assumed to be the direction of propagation (or of the wave vector). This requires an assumption of planarity for the wave structures and also only indicates the direction of the one dominant wave mode for the interval. Furthermore, for regions of nearly linear polarization this method does not work particularly well, since the minimum and intermediate eigenvalues are very similar in such cases [*Song and Russell*, 1999; *Knetter et al.*, 2003; *Hausman et al.*, 2004]. For these reasons, it is important to view with caution any results from MVA analysis, although we retain our results here as first-order approximations for the direction of propagation.

[14] Finally, in order to study the frequency domain of the oscillations, we use wavelet analysis. Wavelet analysis allows us to transform a signal in the time domain into a time-resolved signal in the frequency domain with the time resolution scaled to frequency. *Torrence and Compo* [1998] provide a clear introduction to wavelet analysis and its application to geophysical signals. In our analysis we use the Morlet wavelet with a wave number of six because its shape gives good time localization. We also use a high pass filter to reduce the spectral power due to fluctuations that do not complete at least 3 periods in the time that it takes MGS to travel 500 km. This works out

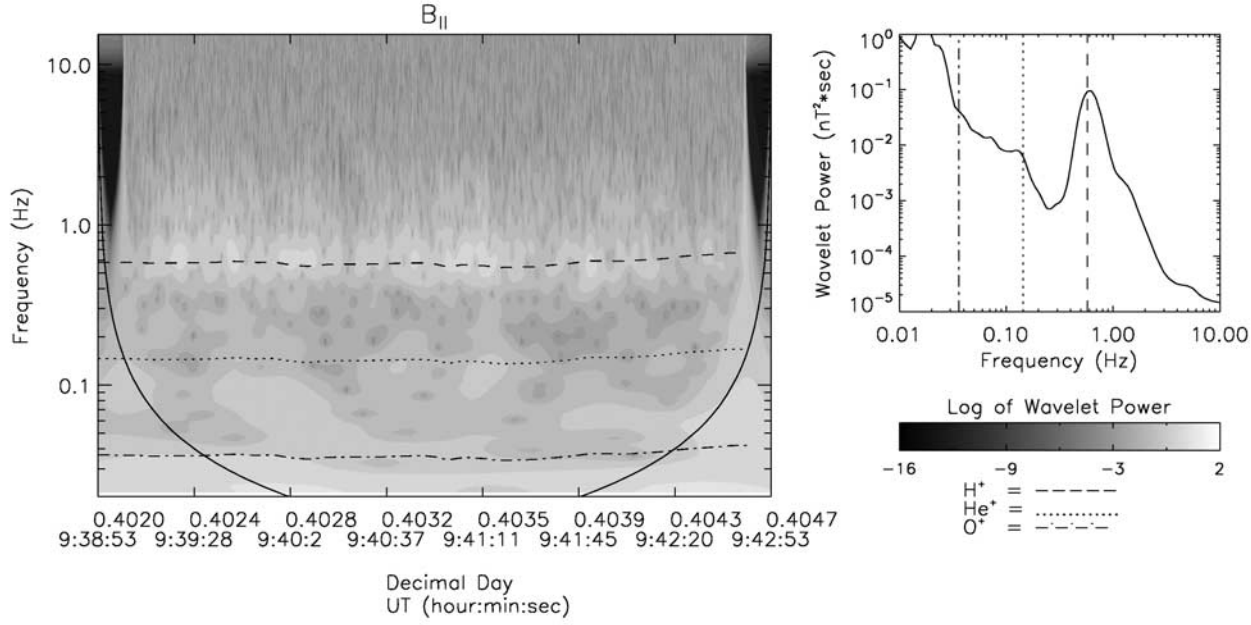

Figure 3. The wavelet spectral analysis of the $B_{||}$ component for the interval shown in Figure 2. The left panel shows the wavelet power spectrum, while the right panel show the global wavelet power spectrum. The dashed lines indicates the average hydrogren gyrofrequency, the dotted lines indicate the helium gyrofrequency, and the dashed-dotted lines indicate the oxygen gyrofrequency. See color version of this figure at back of this issue.

to be approximately 0.02 Hz for the mapping orbits used in this study.

4. Observations

[15] In order to illustrate the oscillations observed during the passage of the solar storm, we select a number of intervals to analyze in depth. Figure 2 shows the first interval chosen, decimal day 303.402 to 303.405. In top left panel, the magnetic field magnitude ($|B|$) for the entire day of 30 October 2003 (decimal day 303) is shown versus time. MGS's passage from the dayside (when $|B|$ is high) to the nightside (when $|B|$ is low) is clearly seen as MGS makes approximately 12 orbits during that day. The main

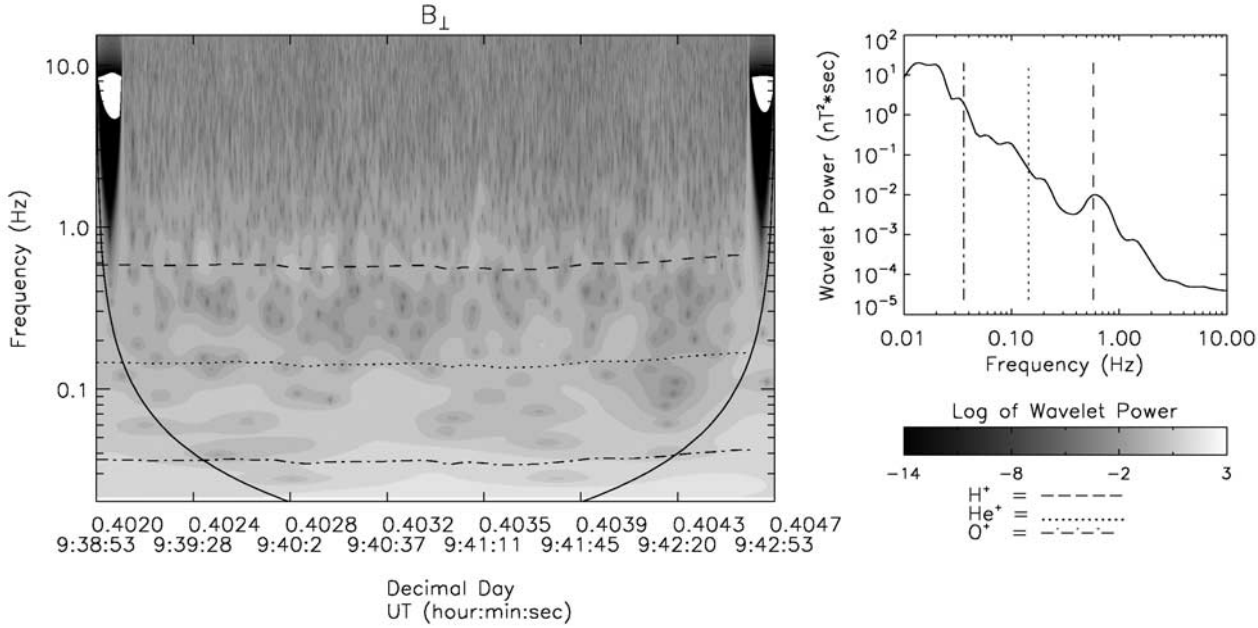

Figure 4. The same as Figure 3 except for the $B_{\perp}$ component. See color version of this figure at back of this issue.

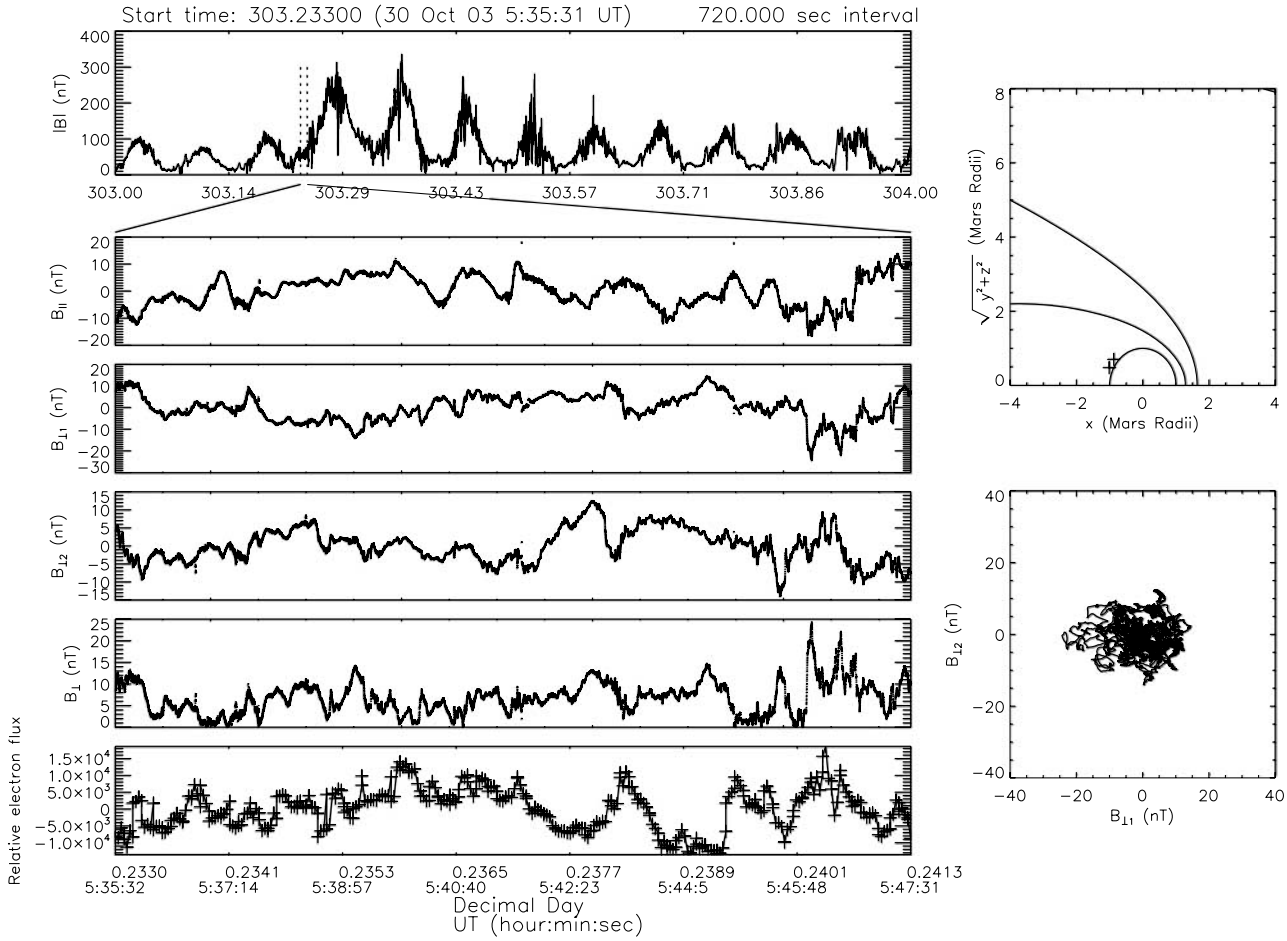

Figure 5. The same as Figure 2 but for the interval of 303.233 to 303.2413.

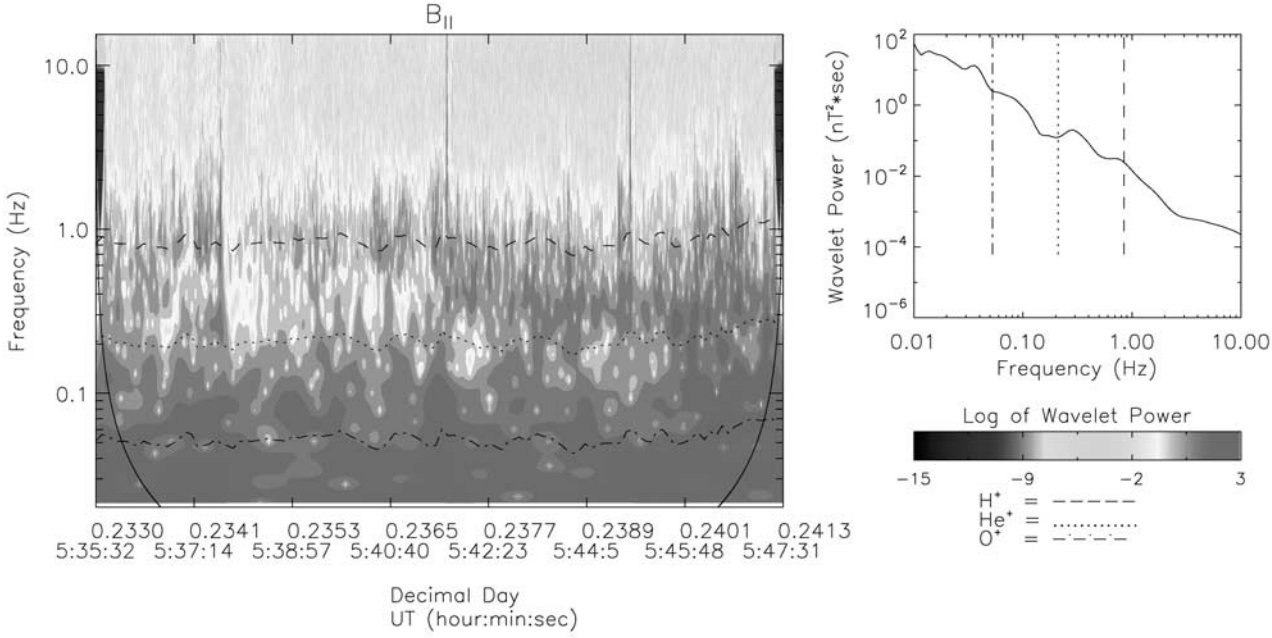

Figure 6. The same as Figure 3 but for the interval of 303.233 to 303.2413. See color version of this figure at back of this issue.

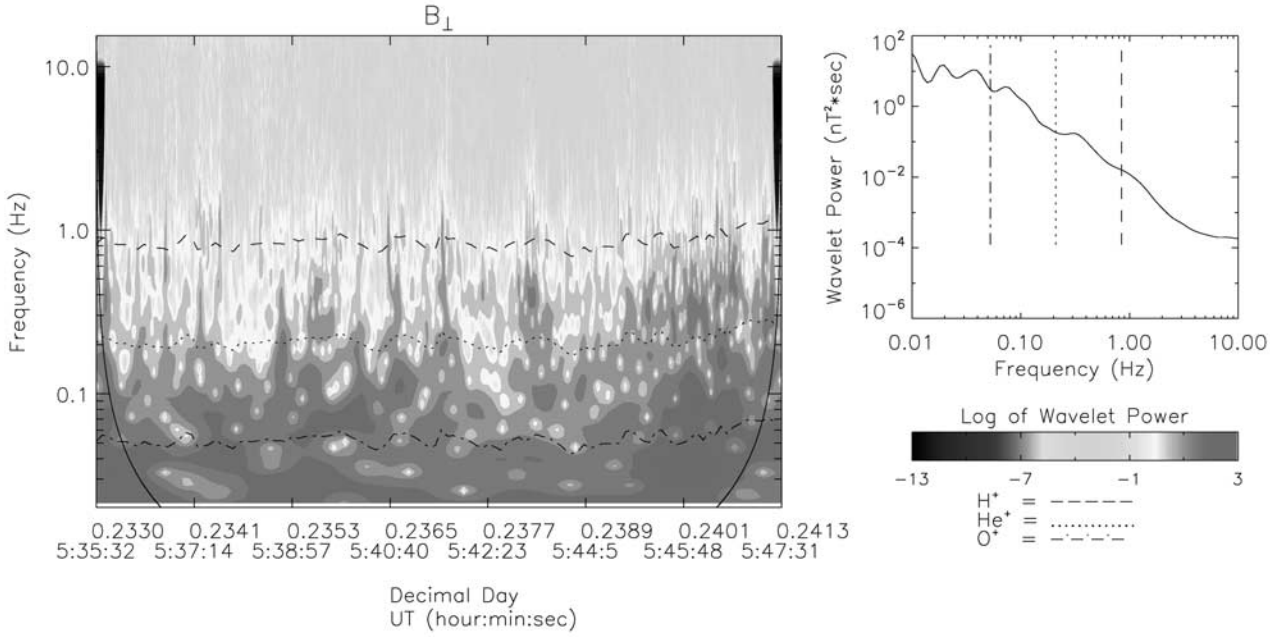

Figure 7. The same as Figure 4 but for the interval of 303.233 to 303.2413. See color version of this figure at back of this issue.

shock wave from the solar storm seems to have hit around 303.2 when $|B|$ increases to well above its normal levels ($|B|$ is normally about 30 nT on the nightside and near 60 nT on the dayside at these altitudes). The panels below the $|B|$ profile show the MF magnetic field components for the region of interest. The last panel on the left shows the relative omnidirectional flux (cm^{-2} s^{-1} sr^{-1} eV^{-1}) of electrons with energies of 191 eV. In the upper right, we show as plus signs the starting and ending locations (which overlap on this scale) of MGS for the interval in SS coordinates. We also show the best fit locations of the bow shock and MPB from *Vignes et al.* [2000]. In the lower right panel, we show the perpendicular components of the magnetic field in MF coordinates plotted versus each other (a hodogram). Figures 3 and 4 show wavelet transforms of approximately the same interval for the $B_{\|}$ and $B_{\perp}$ components, respectively. The left panels show the wavelet power spectra, whereas the right panels show the global (time integrated) wavelet power spectra. The dashed line indicates the average hydrogen gyrofrequency, the dotted line the helium gyrofrequency, and the dashed-dotted line the oxygen gyrofrequency.

[16] During nonstorm periods at this location, far on the nightside at approximately 400 km, the magnetic field is weak and coherent oscillations are almost undetectable (see the third case example). However, in this case (about 5 hours after the main shock wave seems to have hit Mars), the field is relatively high (38 nT) and there is clear spectral power at a variety of frequencies. Most striking is the clear signal at the local hydrogen gyrofrequency (about 0.6 Hz) in the $B_{\|}$ oscillations. This signal is clearly evident in the $B_{\|}$ time series. Spectral power at this frequency is also seen in the $B_{\perp}$ component although it is considerably weaker. Interestingly, there is also spectral power in both components at frequencies lower than the oxygen gyrofrequency (0.04 Hz). This lower-frequency signal exhibits more spectral power in the $B_{\perp}$ component and is evident in a qualitative inspection of that component. It should be noted that these observed frequencies are in the frame of the moving spacecraft. However, since the average velocity of MGS in the mapping orbit is about 4 km/s, it is expected that the Doppler shift from the spacecraft frame to plasma frame should be small.

[17] The hodogram shows that the perpendicular components are quite variable during the interval, although there are periods when they are fairly linearly polarized. The overall ellipticity during the interval is 0.4. Using MVA, the ratio of the intermediate to minimum eigenvalues is 2.5 which when combined with the periods of linear polarization during the interval makes somewhat uncertain the calculated direction of propagation (19° relative to the mean field) for the dominant wave mode. The relative sense of polarization for the interval is −0.02 meaning that the perpendicular components are neither predominately left-handed nor right-handed polarized but are rather a fairly even mix. The correlation coefficient between the relative 191 eV electron flux and the $B_{\|}$ component is 0.47 and between the electron flux and the $B_{\perp}$ component the coefficient is −0.10.

[18] Figures 5, 6, and 7 show plots similar to Figures 2, 3, and 4 for another illustrative interval, decimal day 303.233 to 303.2413. MGS was on the nightside during this interval also. However, this interval is near the time when the main shock from the solar storm was hitting Mars. The mean $|B|$ for the interval is 55 nT, the mean relative polarization is 0.01, the intermediate to minimum MVA eigenvalue ratio is 1.7 (rendering unreliable the calculated 68° propagation angle relative to the mean field), and the total ellipticity is

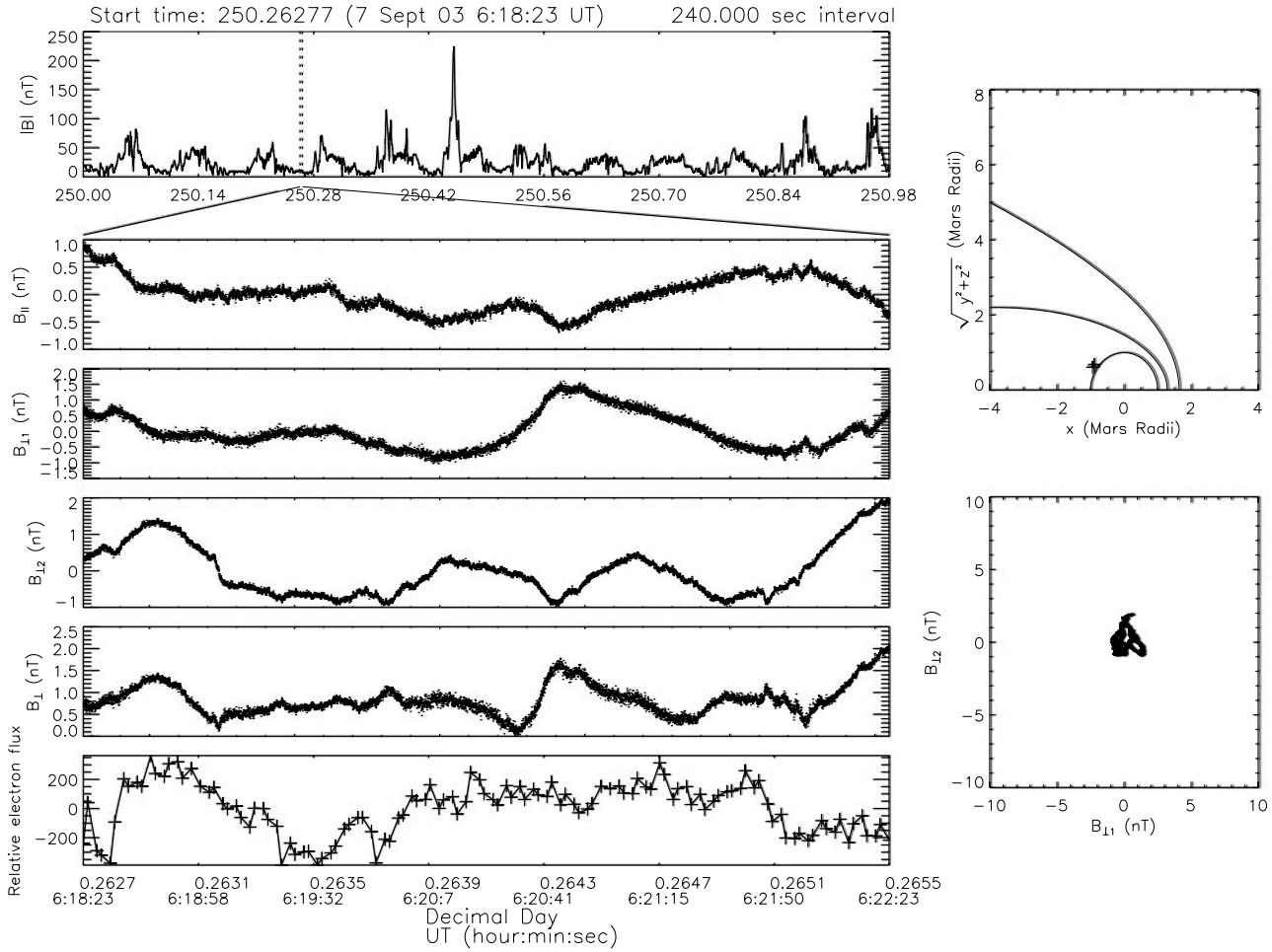

Figure 8. The same as Figure 2 but for the interval 250.263 to 250.266 (7 September 2003). This day showed no signs of unusual solar activity.

0.84 (as seen by the roundness of the hodogram). The correlation coefficients between the relative electron flux and the $B_{\|}$ and $B_{\perp}$ components are 0.32 and -0.24, respectively.

[19] Qualitative inspection of the time series of the magnetic components reveals considerable oscillatory activity at a variety of frequencies. The wavelet power spectra in Figures 6 and 7 confirm this picture. More power at a wider range of frequencies is displayed in the $B_{\|}$ component, although the $B_{\perp}$ component also has considerable power. In both cases, the greatest spectral power is displayed at frequencies at and below the local oxygen gyrofrequency.

[20] To provide contrast with the phenomena observed in the previous two case studies, Figure 8 shows a plot similar to Figure 2 for an interval from a day (7 September 2003 or decimal day 250) showing little evidence of unusual solar activity. On 5 September 2003, according to data publicly available at http://cdaweb.gsfc.nasa.gov, instruments on the Advanced Composition Explorer (ACE) spacecraft measured, in near-Earth space, that the solar wind density was about 4 particles cm^{-3}, the bulk solar wind velocity was about 600 km/s, and the ambient solar wind magnetic field was about 5 nT. The solar wind would have taken approximately 2 days to travel from the Earth to Mars during this time so the conditions just mentioned are likely to have existed in the solar wind near Mars on 7 September. Furthermore, a qualitative inspection of MGS data for the interval from decimal day 250.263 to 250.266 shows that the interval is typical for conditions on the Martian nightside at 400 km. The mean $|B|$ for the interval is 10 nT and very small amplitude (<1 nT) oscillations are noticeable in both the $B_{\|}$ and $B_{\perp}$ components. The expected error in the calibration of the MAG data is estimated to be as high as 0.5 nT on the nightside so we regard with caution such small amplitude oscillations. Both the small size and the irregularity of the oscillations are typical for nonstorm nightside observations, although individual intervals do demonstrate both somewhat larger and somewhat smaller amplitude oscillations.

[21] Figures 9, 10, and 11 show data from our last case example. This interval (decimal day 303.433 to 303.436) is from the dayside MPR at about 60° SZA. Normally, this region exhibits $|B|$ around 45 nT but during the passage of the solar storm this interval shows a $|B|$ of 140 nT. This increase in the magnetic field allows stronger perturbations to develop and we see large oscillations developing in the magnetic components and in the electron fluxes. These oscillations are much clearer than the smaller amplitude oscillations normally seen in this region and, unlike the

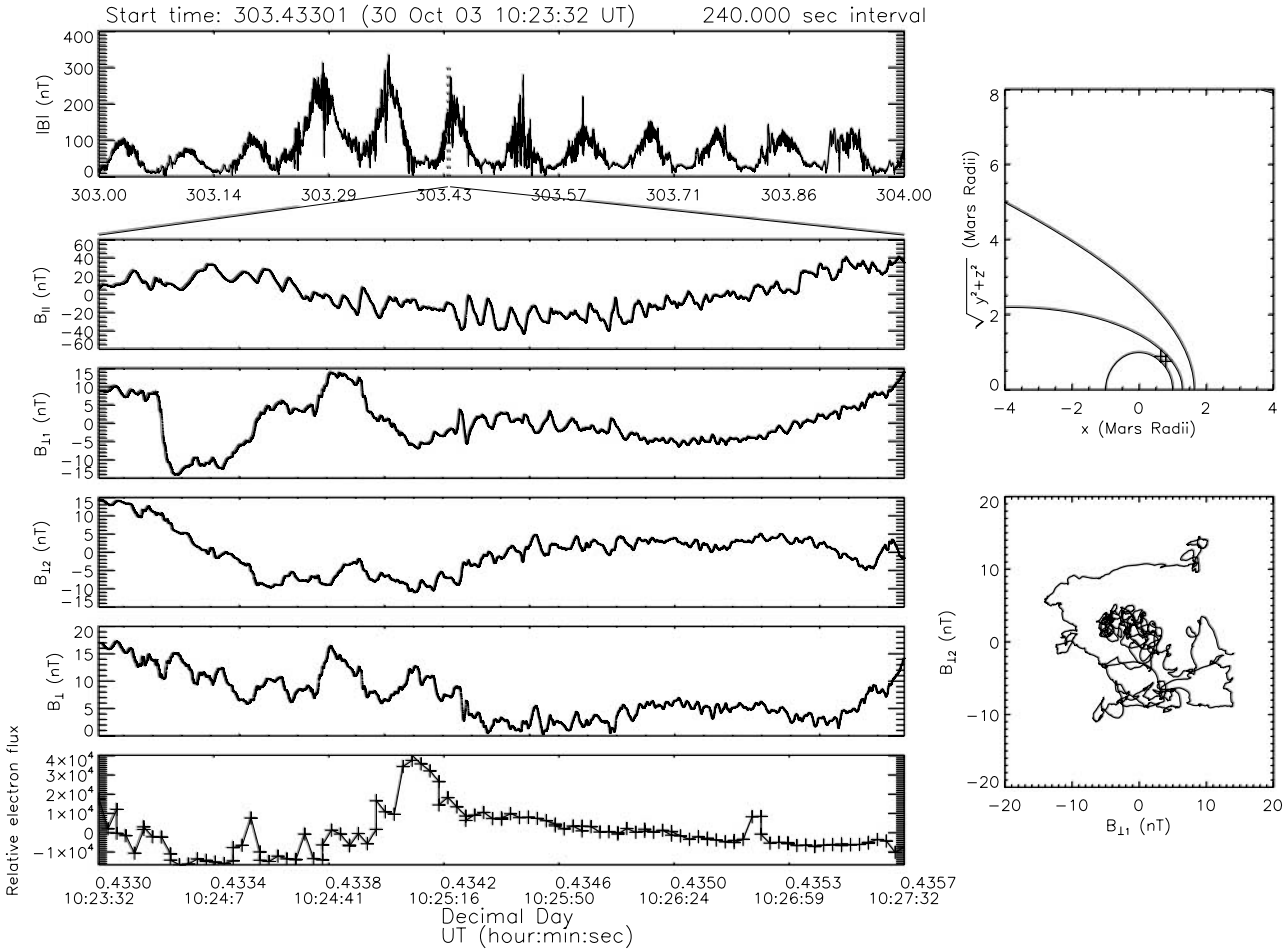

Figure 9. The same as Figure 2 but for the interval of 303.433 to 303.436.

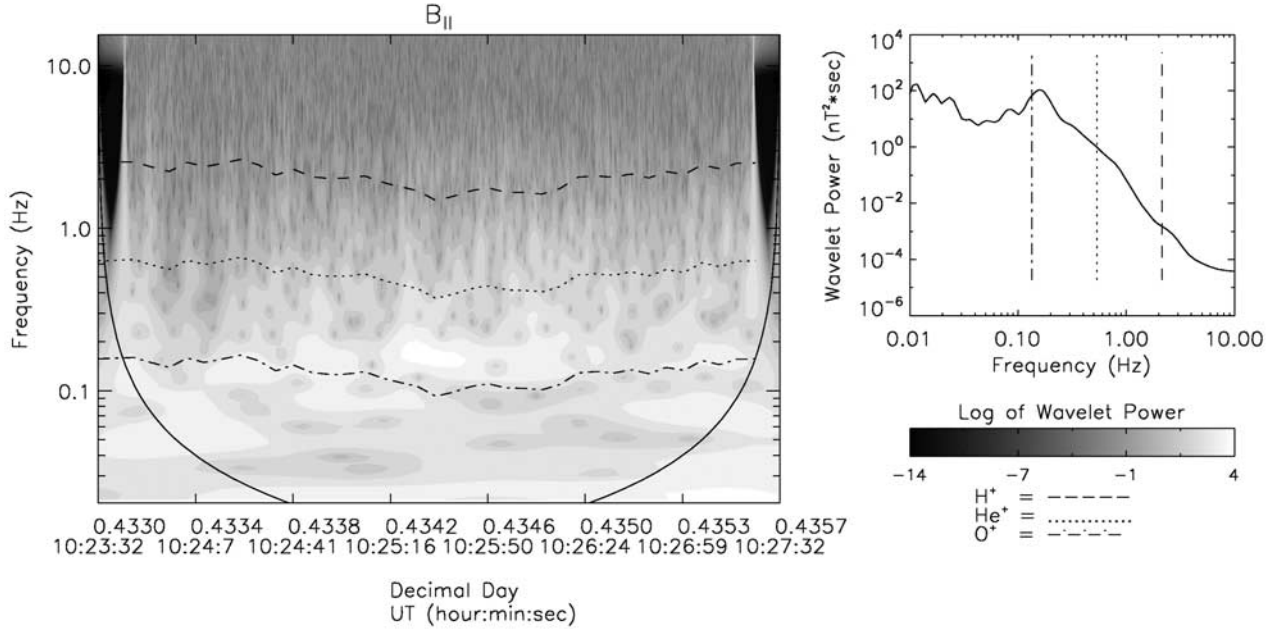

Figure 10. The same as Figure 3 but for the interval of 303.433 to 303.436. See color version of this figure at back of this issue.

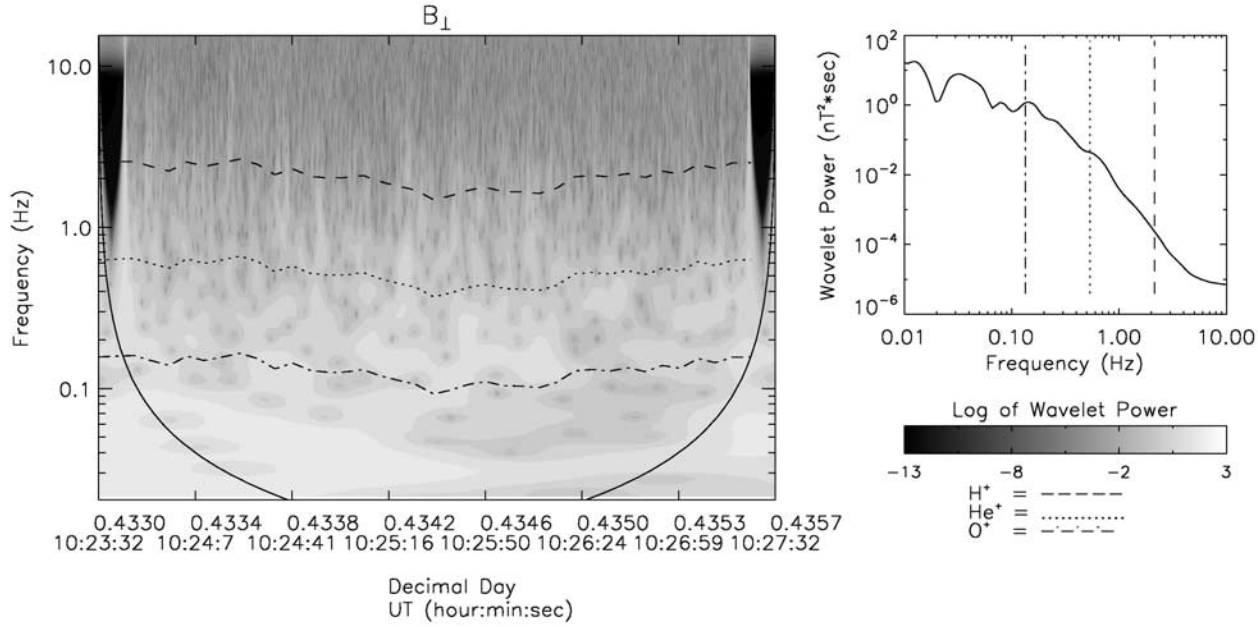

Figure 11. The same as Figure 4 but for the interval of 303.433 to 303.436. See color version of this figure at back of this issue.

previous case studies, show power across many frequencies with no distinct peaks. Spectral power is seen in both the $B_{\|}$ and $B_{\perp}$ components, as is normal for this region, but in this case the $B_{\|}$ oscillations clearly dominate with spectral power at and below the oxygen gyrofrequency being very obvious. Similar examples can be found in dayside data from time periods not during solar storms although with less clarity and smaller amplitude oscillations. The ellipticity for the oscillations during the interval is 0.13, the relative polarization is 0.12, the MVA eigenvalue ratio is 1.2 (again rendering the angle of propation of 87° suspect), the correlation coefficient between the electron flux and the $B_{\|}$ component is −0.64, and the corrrelation coefficient for the electron flux and the $B_{\perp}$ component is −0.22.

5. Discussion

[22] The foregoing case studies and a qualitative examination of other intervals allow us to offer the following summary of our observations. In the dayside MPR at 400 km during normal conditions, oscillatory activity is spread between the $B_{\|}$ and $B_{\perp}$ components although the $B_{\|}$ components often offer greater spectral clarity and power. The greatest spectral power is present at frequencies at or below the hydrogen gyrofrequency. The passage of the solar storm serves to enhance the clarity and regularity of the oscillations, and although they continue to divide their power between components, the oscillations still often show greater spectral power in the $B_{\|}$ component. Individual intervals during the solar storm also are marked by propagation perpendicular to the background field and by anticorrelations between the electron fluxes and the $B_{\|}$ components. These characteristics indicate the likely presence of mirror-mode instabilities since such instabilities exhibit many of the characteristics just enumerated [*Gary*, 1993]. Such instabilities may be generated by temperature anisotropies created as the enhanced solar wind from the solar storm compresses and penetrates the MPB [*Crider et al.*, 2005]. Such conditions may also allow for the convection of the mirror-mode instabilities from the magnetosheath where they have been observed to exist [*Espley et al.*, 2004]. Further work is required to fully understand the physical origin of these instabilities.

[23] On the nightside at 400 km, we find that the general picture during the solar storm is very similar to the day side MPR (although $|B|$ is of course lower) with considerable spectral power divided between the $B_{\|}$ and $B_{\perp}$ components. Individual intervals during the solar storm's passage often show relatively powerful and regular $B_{\|}$ fluctuations (and to a lesser extent $B_{\perp}$ fluctuations) in contrast to the normally quiet conditions in this region. Some intervals show some correlations between the electron and the magnetic components and some intervals show a moderate degree of elliptical polarization. However, the most striking feature is the very clear signal observed mainly in the $B_{\|}$ component at the local proton gyrofrequency observed occasionally during the solar storm. Also, the strong spectral signal at or below the oxygen gyrofrequency is something not normally observable in this region. Unfortunately, a wide variety of plasma wave modes and instabilities have at least some of the characteristics that we observe in the region so identification of a single dominant wave mode is difficult without further measurements. Nonetheless, the clear evidence for spectral power at and below the oxygen gyrofrequency suggests the involvement of oxygen ions and/or heavier species (such as molecules such as O_2^+, CO_2^+, CO^+, and N_2^+) in producing the oscillations observed. Such ions are most likely produced from the planetary neutral atmosphere. Escaping fluxes of such ions have been observed by Phobos 2 [*Lundin et al.*, 1989] and by Mars Express [*Lundin et al.*, 2004].

[24] Likewise, during nonstorm conditions wave activity associated with planetary pickup ions has been observed in the nightside magnetosheath [*Espley et al.*, 2004]. By observing, during the passage of the solar storm, that such wave phenomena also occur in the normally placid tail region, we show that atmospheric loss may occur across a larger spatial region during the passage of solar storms and that therefore enhanced rates of atmospheric loss may occur. This speculation is reinforced by the idea that the powerful compression caused by the passage of the solar storm is expected to cause larger segments of the planetary atmosphere to be exposed to the solar wind and hence subject to pickup mechanisms. It is an interesting question, which we leave to future research, as to the relative magnitudes of the total loss throughout Martian history caused by the steady state interaction with the solar wind versus that caused by the enhanced episodic loss from strong solar activity.

[25] Finally, we mention that in order to more fully understand the physical origin of the oscillations and in order to make a careful comparison with contemporary theory, we would want measurements of the pressures, temperatures, velocities, and densities of the plasma constituents. Fortunately, some of these measurements are available or derivable from observations made by the Mars Express (MEX) spacecraft which recently arrived at Mars [*Lundin et al.*, 2004]. Unfortunately, MEX had not yet arrived at Mars at the time of the solar storm examined in this work nor does it carry a magnetometer. Nonetheless, if similar solar storms arrive at Mars during MEX's lifetime (as previously noted the storm studied in this report was exceptionally large but significant if somewhat smaller solar storms are common on decadal timescales) then it should be possible to make intercomparisons between the MGS MAG/ER data and relevant MEX data from similar altitudes. We look forward to this opportunity and to also further study of interesting intervals from our current data set which were omitted for the sake of brevity in this report. Such studies will further our understanding of the physics involved in the passage of a large solar storm at Mars.

[26] **Acknowledgments.** We are grateful for useful discussions with J. E. P. Connerney, V. Delouille, C. Knez, P. Lawton, and C. Lemon. The wavelet analysis software used in this work was based on software provided by C. Torrence and G. Compo and is available at http://paos.colorado.edu/research/wavelets/. We thank N. Ness at the Bartol Institute, D. J. McComas at SwRI, the ACE Science Center, and CDAWeb for providing the ACE data. This research was supported by the NASA GSRP program under grant number NGT5-156.

[27] Arthur Richmond thanks Richard Lundin and David Mitchell for their assistance in evaluating this paper.

References

Acuña, M. H., et al. (1998), Magnetic field and plasma observations at Mars: Initial results from the Mars Global Surveyor Mission, *Science*, *279*, 1676–1680.

Acuña, M. H., et al. (2001), Magnetic field of Mars: Summary of results from the aerobraking and mapping orbits, *J. Geophys. Res.*, *106*, 23,403–23,417.

Albee, A. L., R. E. Arvidson, F. Palluconi, and T. Thorpe (2001), Overview of the Mars Global Surveyor mission, *J. Geophys. Res.*, *106*, 23,291–23,316.

Cloutier, P. A., et al. (1999), Venus-like interaction of the solar wind with Mars, *Geophys. Res. Lett.*, *26*, 2685–2688.

Crider, D. H., et al. (2000), Evidence of electron impact ionization in the magnetic pileup boundary of Mars, *Geophys. Res. Lett.*, *27*, 45–48.

Crider, D. H., D. Vignes, A. M. Krymskii, T. K. Breus, N. F. Ness, D. L. Mitchell, J. A. Slavin, and M. Acuña (2003), A proxy for determining solar wind dynamic pressure at Mars using Mars Global Surveyor data, *J. Geophys. Res.*, *108*(A12), 1461, doi:10.1029/2003JA009875.

Crider, D. H., J. R. Espley, D. A. Brain, D. L. Mitchell, J. E. P. Connerney, and M. H. Acuña (2005), Mars Global Surveyor observations of the October 2003 solar super-storm's encounter with Mars, *J. Geophys. Res.*, doi:10.1029/2004JA010881, in press.

Espley, J. R., P. A. Cloutier, D. A. Brain, D. H. Crider, and M. H. Acuña (2004), Observations of low-frequency magnetic oscillations in the Martian magnetosheath, magnetic pileup region, and tail, *J. Geophys. Res.*, *109*, A07213, doi:10.1029/2003JA010193.

Gary, S. P. (1993), *Theory of Space Plasma Microinstabilities*, Cambridge Univ. Press, New York.

Hausman, B. A., F. C. Michel, J. R. Espley, and P. A. Cloutier (2004), On determining the nature and orientation of magnetic directional discontinuities: Problems with the minimum variance method, *J. Geophys. Res.*, *109*, A11102, doi:10.1029/2004JA010670.

Knetter, T., F. M. Neubauer, T. Horbury, and A. Balogh (2003), Discontinuity observations with Cluster, *Adv. Space Res.*, *32*, 543.

Lundin, R., A. Zakharov, R. Pellinen, H. Borg, B. Hultqvist, N. Pissarenko, E. M. Dubinin, S. W. Barabash, I. Liede, and H. Koskinen (1989), First measurements of the ionospheric plasma escape from Mars, *Nature*, *341*, 609–612.

Lundin, R., et al. (2004), Solar Wind-Induced Atmospheric Erosion at Mars: First Results from ASPERA-3 on Mars Express, *Science*, *305*, 1933–1936.

Mitchell, D. L., R. P. Lin, H. Reme, D. H. Crider, P. A. Cloutier, J. E. P. Connerney, M. H. Acuña, and N. F. Ness (2000), Oxygen Auger electrons observed in Mars' ionosphere, *Geophys. Res. Lett.*, *27*, 1871–1874.

Press, W. H., S. A. Teukolsky, W. T. Vetterling, and B. P. Flannery (1992), Statistical description of data, in *Numerical Recipes in Fortran*, 2nd ed., 963 pp., chap. 14, Cambridge Univ. Press, New York.

Song, P., and C. T. Russell (1999), Time series data analyses in space physics, *Space Sci. Rev.*, *87*, 387–463.

Torrence, C., and G. P. Compo (1998), A practical guide to wavelet analysis, *Bull. Am. Meteorol. Soc.*, *79*, 61–78.

Vignes, D., C. Mazelle, H. Reme, M. H. Acuña, J. E. P. Connerney, R. P. Lin, D. L. Mitchell, P. A. Cloutier, D. H. Crider, and N. F. Ness (2000), The solar wind interaction with Mars: Locations and shapes of the bow shock and magnetic pile-up boundary from the observations of the MAG/ER experiment onboard Mars Global Surveyor, *Geophys. Res. Lett.*, *27*, 49–52.

M. H. Acuña, NASA Goddard Space Flight Center, Code 695.0, Greenbelt, MD 20701, USA. (mario.acuna@gsfc.nasa.gov)

D. A. Brain, Space Sciences Laboratory, University of California, Berkeley, 7 Gauss Way, Berkeley, CA 94720-7450, USA. (brain@ssl.berkeley.edu)

P. A. Cloutier and J. R. Espley, Department of Physics and Astronomy, MS-108, Rice University, Houston, TX 77005, USA. (pac@spacibm.rice.edu; espley@rice.edu)

D. H. Crider, Catholic University of America, c/o 106 Driftwood Dr., Gibsonville, NC 27249, USA. (dcrider@lepvax.gsfc.nasa.gov)

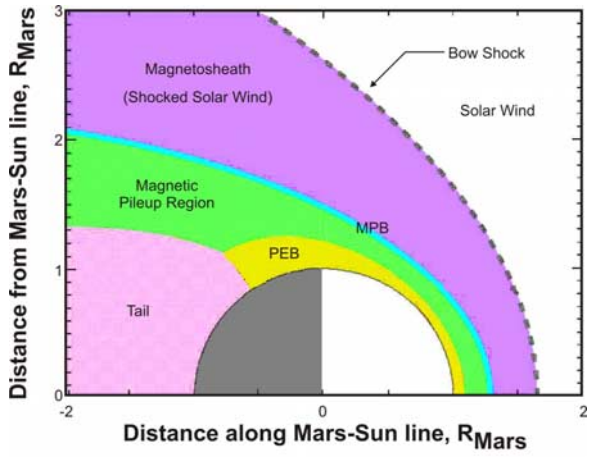

Figure 1. A schematic diagram (approximately to scale) illustrating the regions of the Martian interaction with the solar wind. Not shown are the complications introduced by the crustal magnetic field sources. The MPB is the magnetic pileup boundary and the PEB is the photoelectron boundary. Adapted from *Crider et al.* [2003].

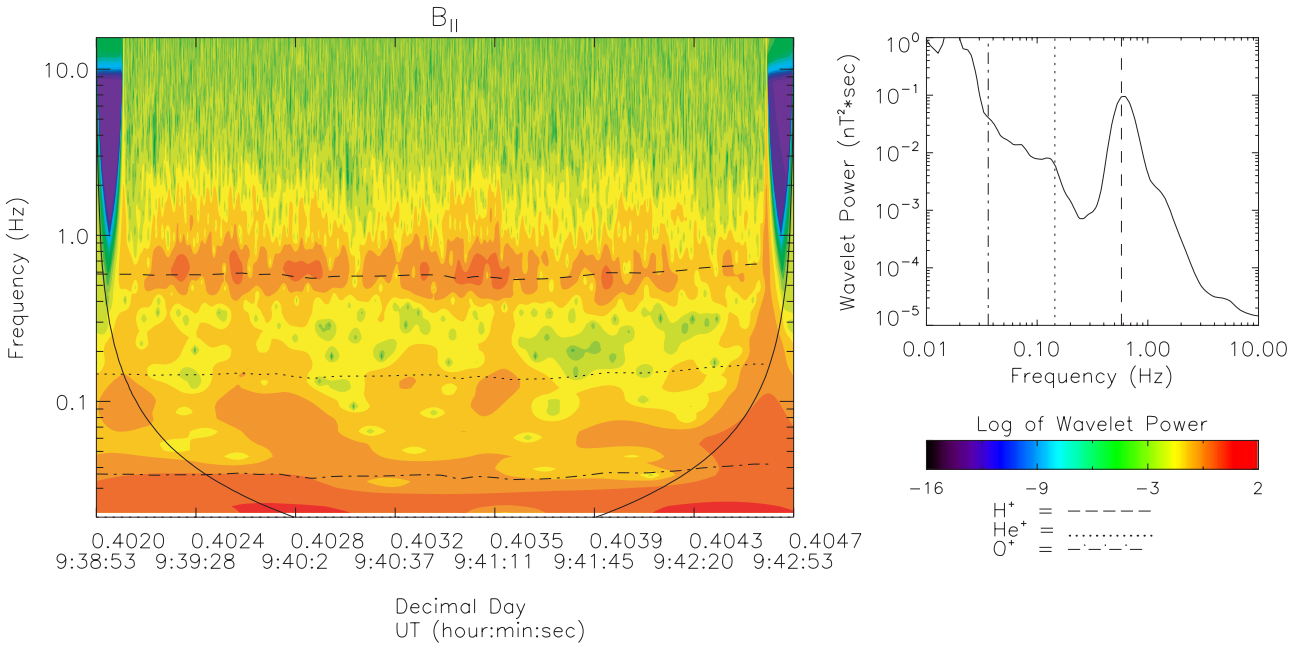

Figure 3. The wavelet spectral analysis of the $B_{||}$ component for the interval shown in Figure 2. The left panel shows the wavelet power spectrum, while the right panel show the global wavelet power spectrum. The dashed lines indicates the average hydrogren gyrofrequency, the dotted lines indicate the helium gyrofrequency, and the dashed-dotted lines indicate the oxygen gyrofrequency.

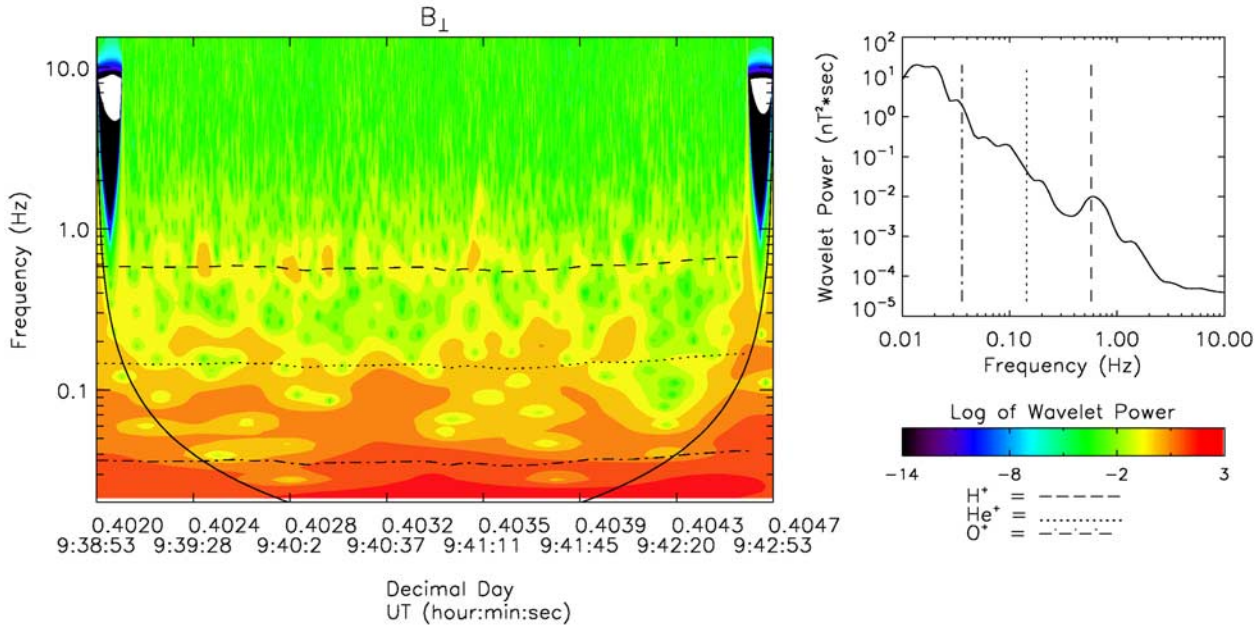

Figure 4. The same as Figure 3 except for the $B_\perp$ component.

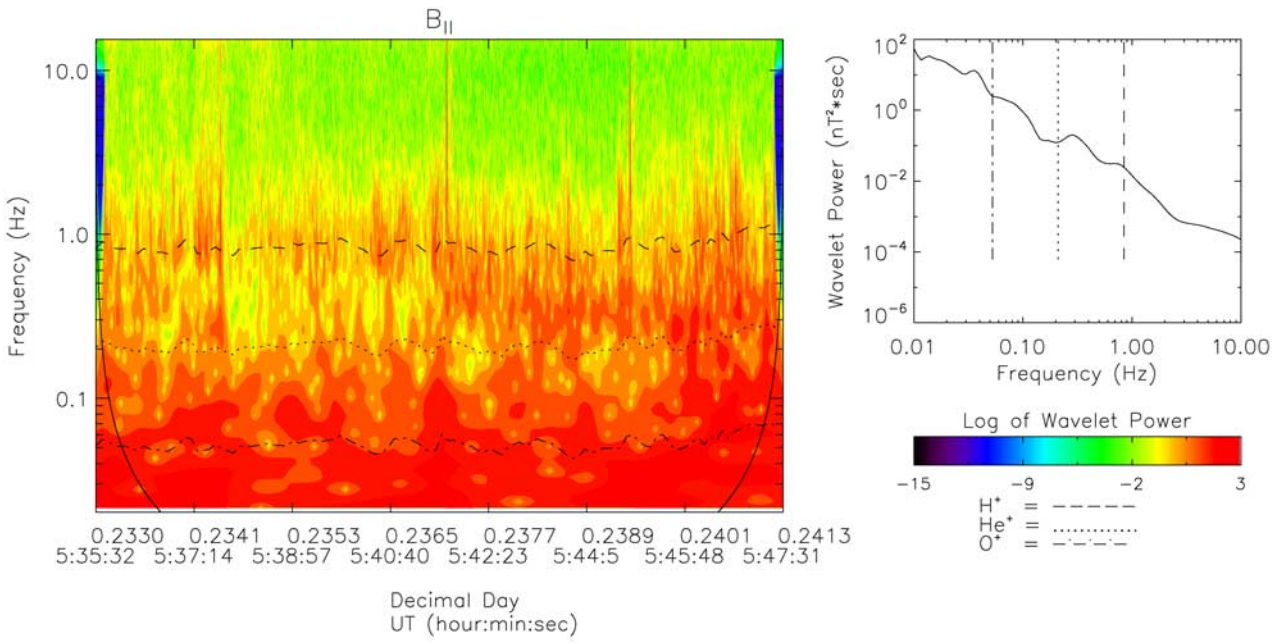

Figure 6. The same as Figure 3 but for the interval of 303.233 to 303.2413.

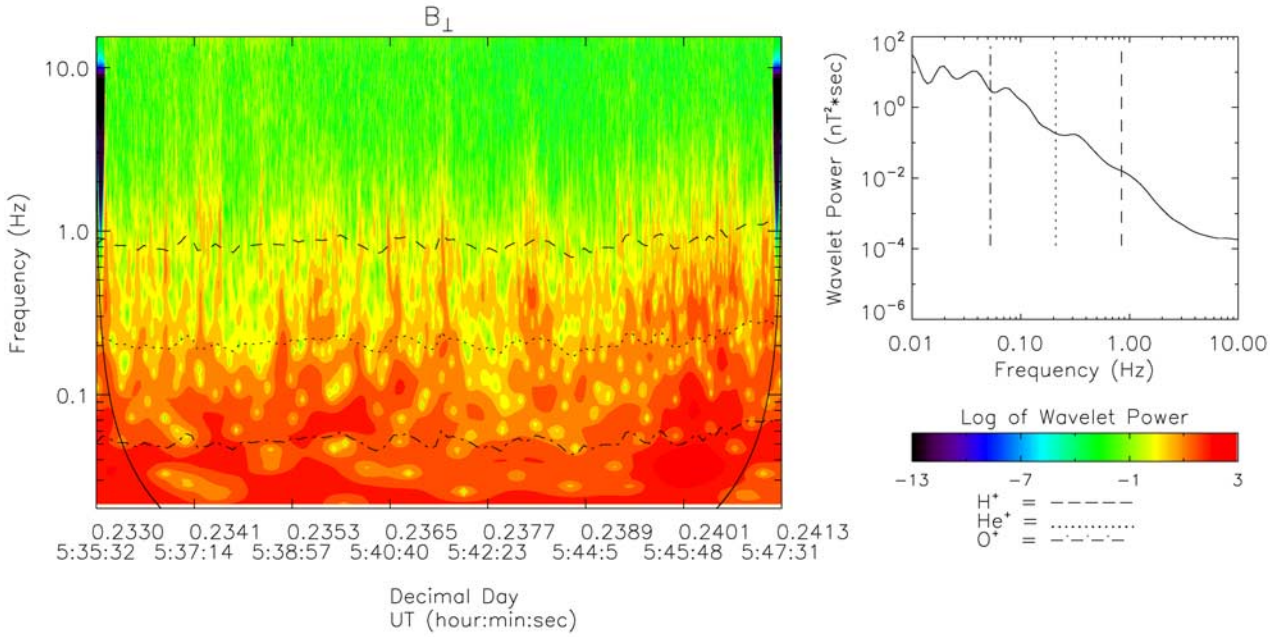

Figure 7. The same as Figure 4 but for the interval of 303.233 to 303.2413.

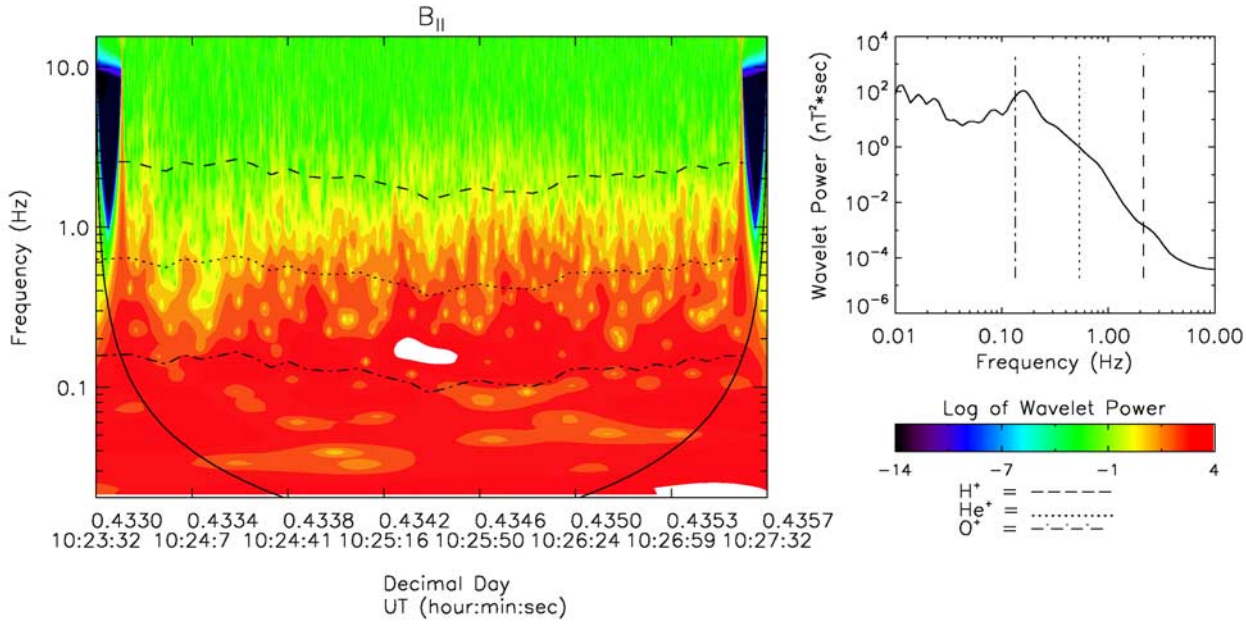

Figure 10. The same as Figure 3 but for the interval of 303.433 to 303.436.

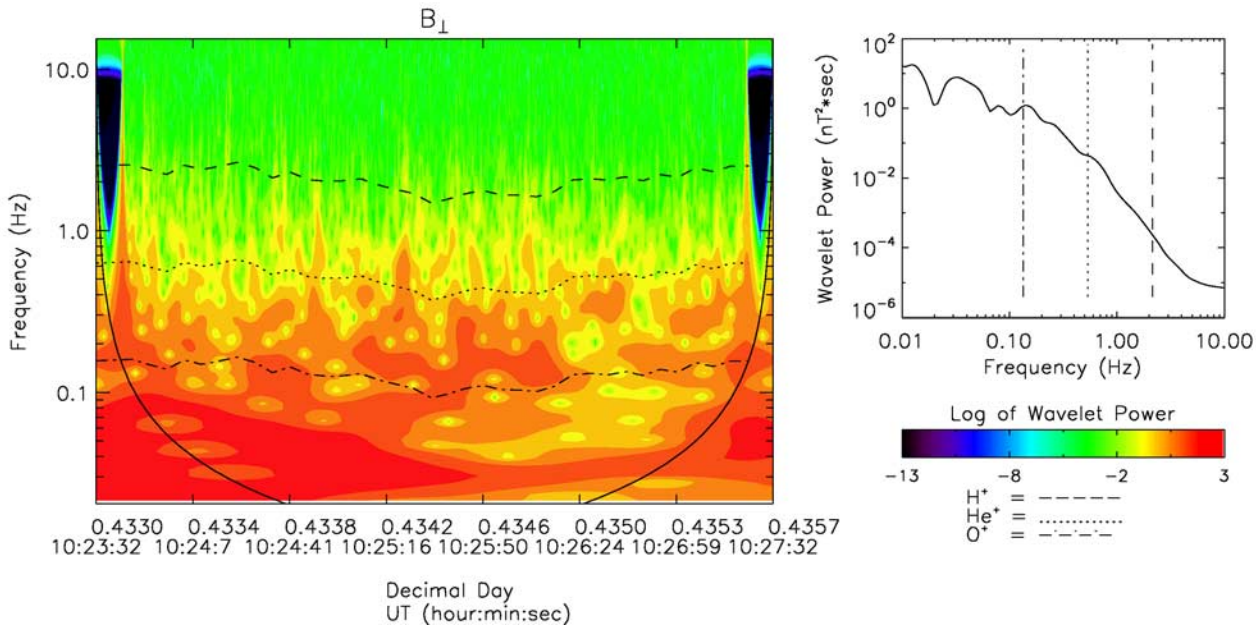

Figure 11. The same as Figure 4 but for the interval of 303.433 to 303.436.